Both differential and equatorial heating contributed to African monsoon variations during the mid-Holocene Supporting Information

Ori Adam[a,*], Tapio Schneider[b], Yehouda Enzel[a], Jay Quade[c]

[a] *The Institute of Earth Sciences, The Hebrew University of Jerusalem, Givat Ram, Jerusalem 91904, Israel*
[b] *California Institute of Technology, 1200 E. California Blvd., Pasadena, CA 91125, USA*
[c] *Department of Geosciences, University of Arizona, 1040 E. 4th Street, Tucson, AZ 85721, USA*

Supporting Information (SI)

The following supporting information provides:

1. A derivation of Eq. (4) for fractional changes on the position of the ITCZ;
2. An empirical regression model for absolute changes in ϕ_{ITCZ};
3. Model-specific and ensemble-mean plots of changes between the mid-Holocene and preindustrial conditions (piControl) in simulations by the 12 PMIP3 climate models analyzed in this study.

1. Derivation of Eq. (4)

Let fractional change be defined as the change in some quantity, $\Delta(\ )$, divided by the unchanged quantity (for example, the fractional change in ϕ_{EFE} is defined as $\delta\phi_{\text{EFE}} \equiv \Delta\phi_{\text{EFE}}/\phi_{\text{EFE}}$). The energy flux equator equation is given by

$$\phi_{\text{EFE}} = -\frac{1}{a}\frac{\text{AET}_0}{\text{I}_0}, \tag{1}$$

changes in ϕ_{EFE} are therefore given by [1]

$$\Delta\phi_{\text{EFE}} = -\frac{1}{a}\left(\frac{\Delta\text{AET}_0}{\text{I}_0} - \frac{\text{AET}_0\Delta\text{I}_0}{(\text{I}_0)^2}\right). \tag{2}$$

*Corresponding author
Email address: ori.adam@mail.huji.ac.il (Ori Adam)

Dividing through by ϕ_{EFE} from Eq. [1] gives

$$\frac{\Delta\phi_{\text{EFE}}}{\phi_{\text{EFE}}} = \frac{\Delta\text{AET}_0}{\text{AET}_0} - \frac{\Delta\text{I}_0}{\text{I}_0} \tag{3}$$

and hence,

$$\delta\phi_{\text{EFE}} = \delta\text{AET}_0 - \delta\text{I}_0. \tag{4}$$

2. Empirical regression model for absolute changes in ϕ_{ITCZ}

The empirical regression model for ϕ_{ITCZ} (Eq. [6] in the main text) can be written in terms of the absolute change,

$$\Delta\phi_{\text{ITCZ}} = \tilde{\alpha_0}\Delta\text{AET}_0 + \tilde{\alpha_1}\Delta\text{NEI}_0 + \tilde{\epsilon}. \tag{5}$$

To test for the robustness of the model, the coefficients $\tilde{\alpha_0}$ and $\tilde{\alpha_1}$ were calculated for each model from the climatological seasonal cycle during the mid-Holocene and preindustrial conditions. As shown in Fig. S6, the regression coefficient $\tilde{\alpha_0}$ is nearly identical in both climates whereas $\tilde{\alpha_1}$ can vary considerably between the two climates (but retains its sign). In addition, as shown in Fig. S7, relative to preindustrial or present-day conditions, a fractional change in NEI_0 of about 50% over Africa corresponds to a relatively small absolute change of $\sim$10 Wm^{-2}.

3. Mid-Holocene and preindustrial conditions in PMIP3 models

Fig. S1 shows the change in precipitation during boreal summer (July–September) between the mid-Holocene and preindustrial conditions. A poleward shift of the tropical rain belt is consistently seen in all models along the Atlantic, Africa and South Asia [2].

As in the African sector, the change between the mid-Holocene and preindustrial simulations in the total atmospheric NEI throughout the tropics during boreal summer is dominated by vertical NEI, shown in Fig S2. The vertical NEI,

in turn, is equal to the sum of net downward radiative fluxes at the top of the atmosphere (Fig. S3) and net upward surface fluxes (S4), which are dominated by ocean heat uptake (changes in upward surface energy fluxes are negligible over land so that the changes in the surface energy balance are dominated by ocean heat uptake).

Figure S5 shows the ensemble-mean change in annual-mean sea surface temperature between the mid-Holocene and preindustrial conditions. The evident equatorial cooling and extratropical warming are associated with the increased obliquity during the mid Holocene [e.g., 3].

References

[1] T. Bischoff, T. Schneider, Energetic constraints on the position of the Intertropical Convergence Zone, J. Climate 27 (2014) 4937–4951. doi:10.1175/JCLI-D-13-00650.1.

[2] P. Braconnot, S. P. Harrison, M. Kageyama, P. J. Bartlein, V. Masson-Delmotte, A. Abe-Ouchi, B. Otto-Bliesner, Y. Zhao, Evaluation of climate models using palaeoclimatic data, Nature Climate Change 2 (2012) 417–424.

[3] G. Lohmann, M. Pfeiffer, T. Laepple, G. Leduc, J. Kim, A model-data comparison of the holocene global sea surface temperature evolution, Climate of the Past 9 (4) (2013) 1807–1839. doi:10.5194/cp-9-1807-2013.

[4] D. Dee, S. M. Uppala, A. J. Simmons, P. Berrisford, P. Poli, S. Kobayashi, U. Andrae, M. Balmaseda, G. Balsamo, P. Bauer, P. B. A.C.M., Beljaars, L. van de Berg, J. B. N., Bormann, C. Delsol, R. Dragani, M. Fuentes, A. Geer, L. Haimberger, S. Healy, H. Hersbach, E. Holm, L. Isaksen, P. Kallberg, M. Kohler, M. Matricardi, A. McNally, B. Monge-Sanz, J.-J. Morcrette, B.-K. Park, C. Peubey, P. de Rosnay, C. Tavolato, J.-N. Thepaut, F. Vitart, The ERA-Interim reanalysis: configuration and performance of the data assimilation system, Quart. J. Roy. Meteor. Soc 137 (2011) 553–597.

[5] K. E. Trenberth, Using atmospheric budgets as a constraint on surface fluxes, J. Climate 10 (1997) 2796–2809. doi:10.1175/1520-0442(1997)010,2796:UABAAC.2.0.CO;2.

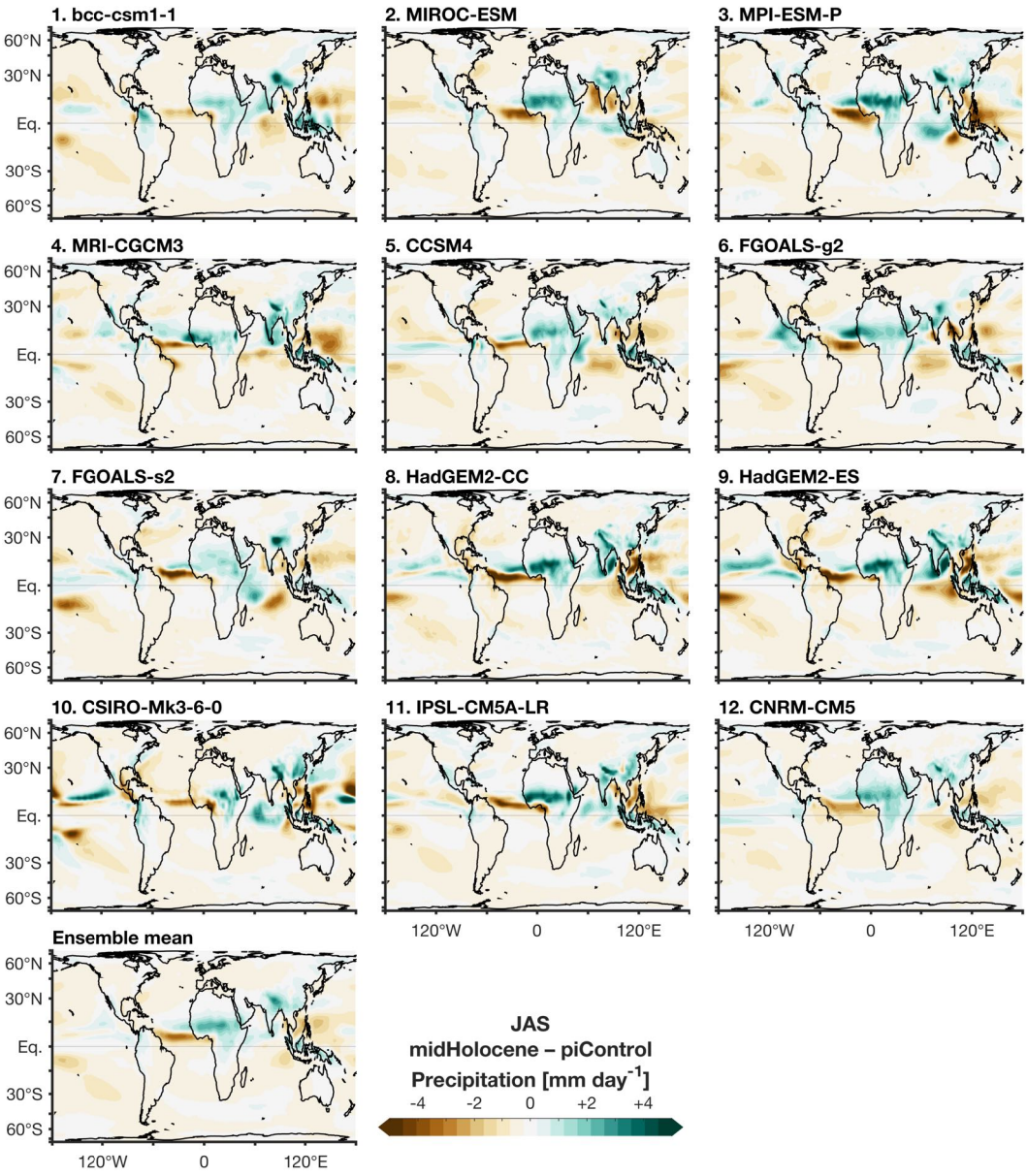

Figure S1: Change in global precipitation during northern summer (July–September) between the mid-Holocene and preindustrial conditions in the 12 PMIP3 models analyzed in this study and in their ensemble mean.

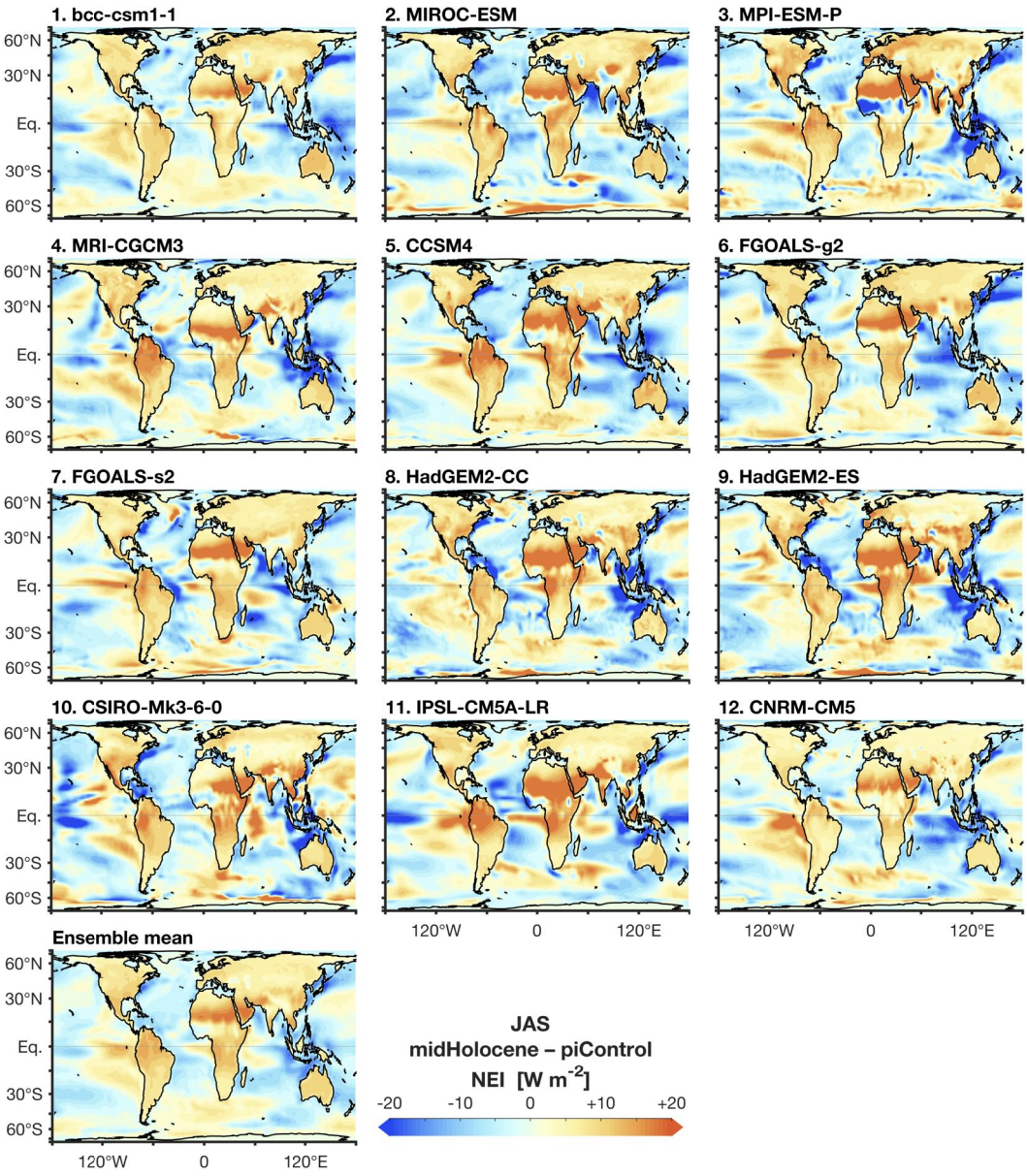

Figure S2: Change in vertical (i.e., from top of the atmosphere and the surface) atmospheric net energy input (NEI) during northern summer (July–September) between the mid-Holocene and preindustrial conditions in the 12 PMIP3 models analyzed in this study and in their ensemble mean.

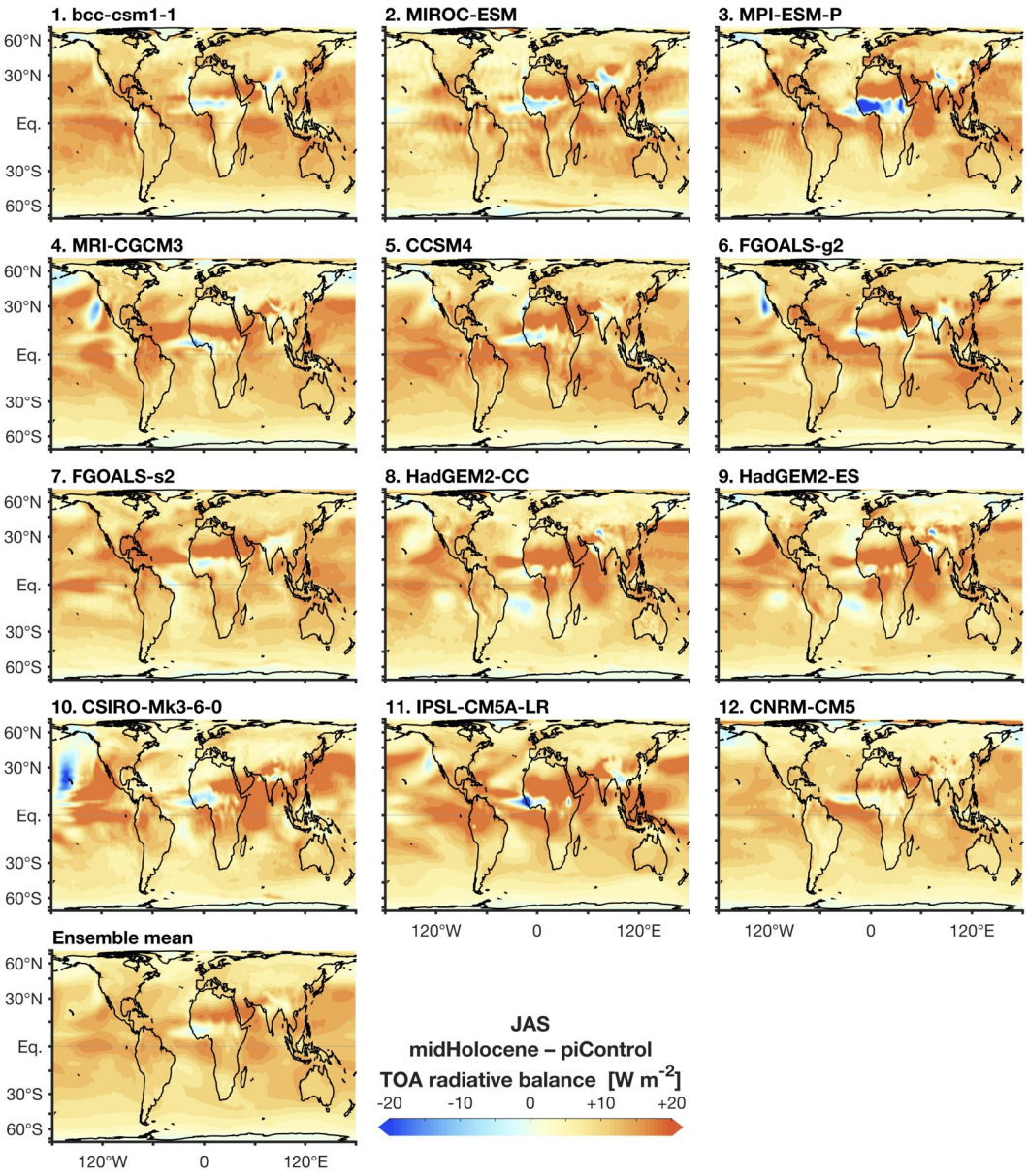

Figure S3: Change in top-of-atmosphere (TOA) net radiative input during northern summer (July–September) between the mid-Holocene and preindustrial conditions in the 12 PMIP3 models analyzed in this study and in their ensemble mean.

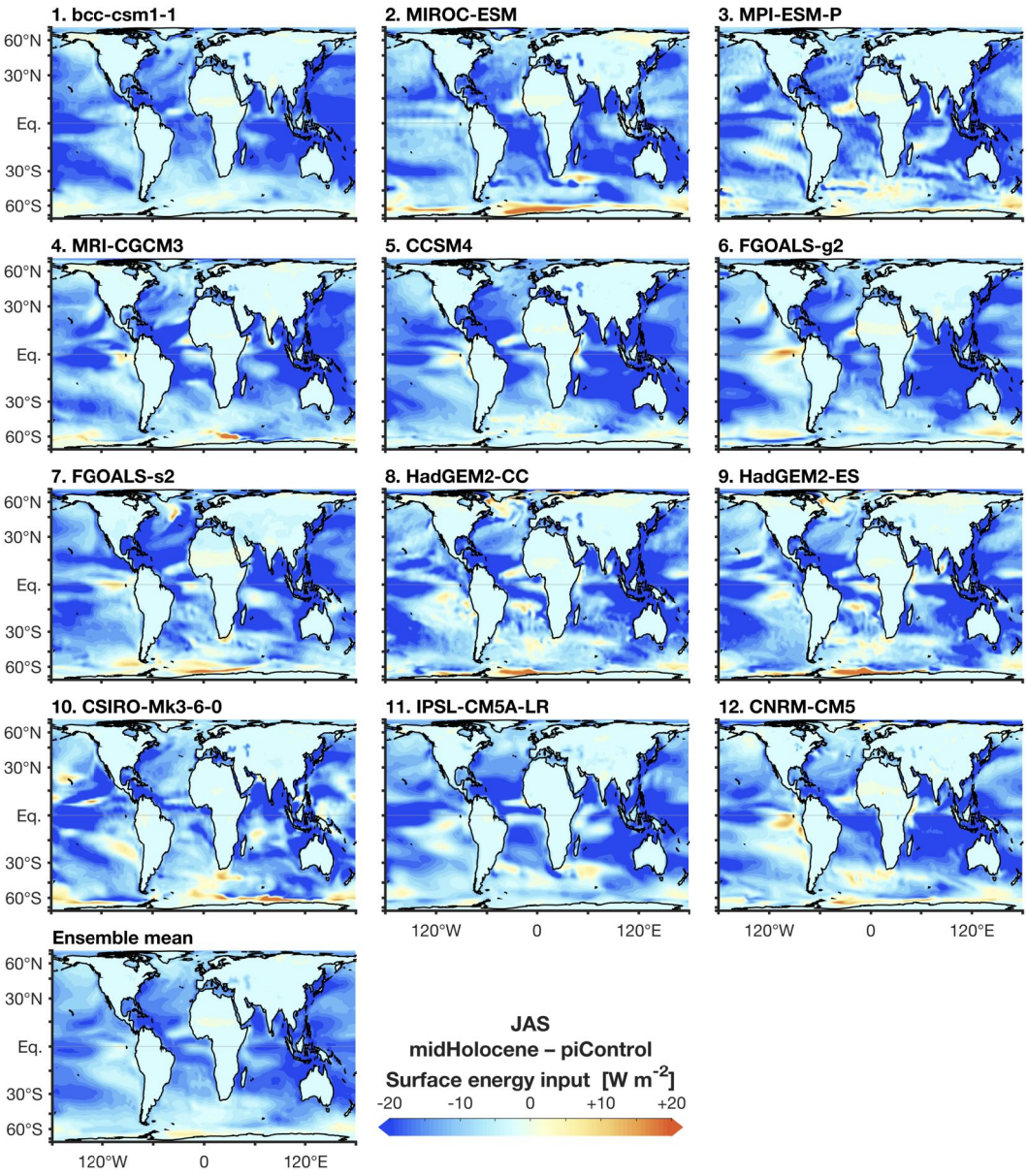

Figure S4: Change in upward surface energy flux during northern summer (July–September) between the mid-Holocene and preindustrial conditions in the 12 PMIP3 models analyzed in this study and in their ensemble mean.

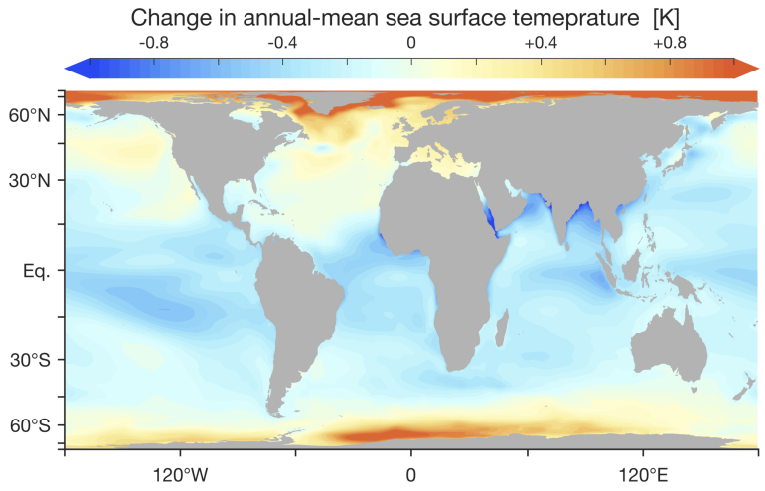

Figure S5: The ensemble mean of the change in annual-mean sea surface temperature (SST) between the mid-Holocene and preindustrial conditions.

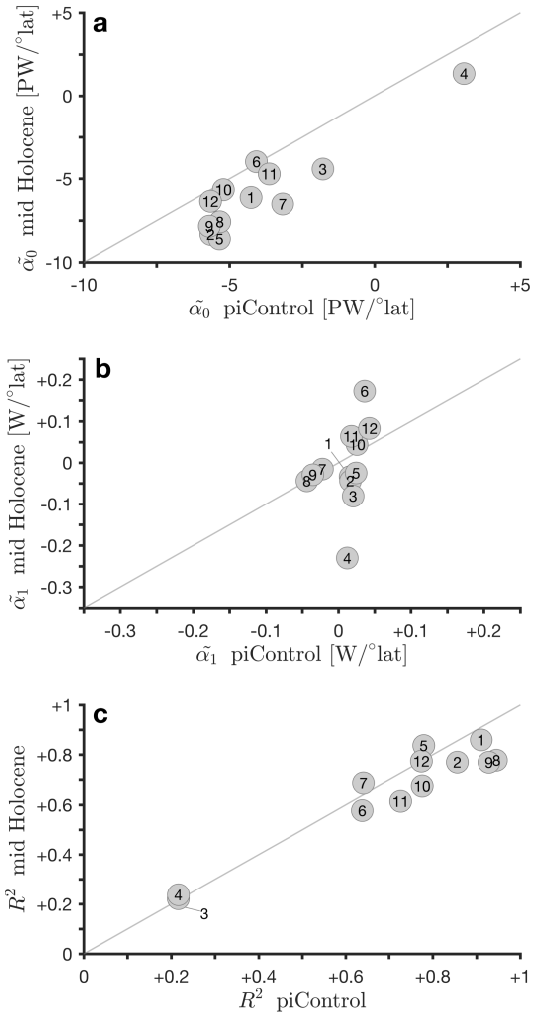

Figure S6: A comparison of the regression coefficients $\tilde{\alpha_0}$ (**a**) and $\tilde{\alpha_1}$ (**b**) and R^2 (**c**) of the regression model $\Delta\phi_{\mathrm{EFE}} = \tilde{\alpha_0}\Delta\mathrm{AET}_0 + \tilde{\alpha_1}\Delta\mathrm{NEI}_0 + \tilde{\epsilon}$, derived from the seasonal cycle for each model during the mid-Holocene and preindustrial conditions. The identity line is shown in gray. Model numbers are as in Fig. 1 of the main text.

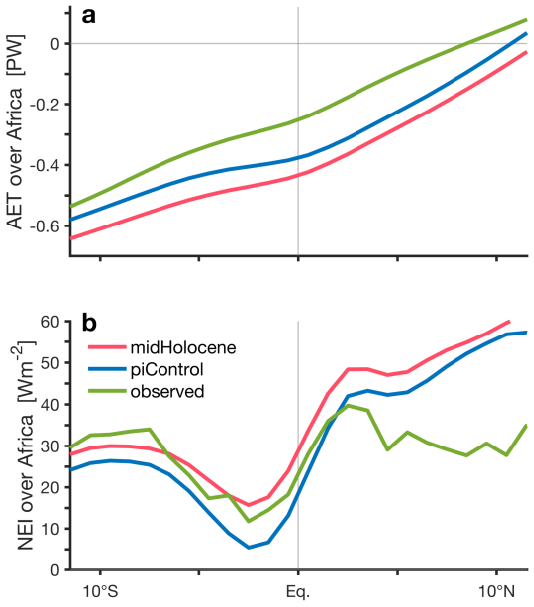

Figure S7: Ensemble-mean atmospheric energy transport (AET, **a**) and net energy input (NEI, **b**) over Africa (20°W–40°E) for the mid-Holocene (red) and preindustrial conditions (blue), and from present day observations (green) during boreal summer (July–September). Present day data was taken from the European Centre for Medium-Range Weather Forecasts (ECMWF) interim reanalysis for 1979–2012 [4], and was corrected for mass balance following the procedure outlined in [5].